Tumor and Stem Cell Biology

Cancer Research

Generation of Prostate Tumor–Initiating Cells Is Associated with Elevation of Reactive Oxygen Species and IL-6/STAT3 Signaling

Yi Qu[1], Anne Margrete Oyan[1,4], Runhui Liu[8], Yaping Hua[1,8], Jigang Zhang[8], Randi Hovland[6], Mihaela Popa[7], Xiaojun Liu[1,8], Karl A. Brokstad[2], Ronald Simon[9], Anders Molven[1,5], Biaoyang Lin[10,11,12], Wei-dong Zhang[8], Emmet McCormack[3], Karl-Henning Kalland[1,4], and Xi-Song Ke[1]

Abstract

How prostate cancer is initiated remains a topic of debate. In an effort to establish a human model of prostate carcinogenesis, we adapted premalignant human prostate EPT2-D5 cells to protein-free medium to generate numerous tight prostate spheres (D5HS) in monolayer culture. In contrast to EPT2-D5 cells, the newly generated D5HS efficiently formed large subcutaneous tumors and subsequent metastases *in vivo*, showing the tumorigenicity of D5HS spheres. A striking production of interleukin (IL)-6 mRNA and protein was found in D5HS cells. The essential roles of IL-6 and the downstream STAT3 signaling in D5HS tumor sphere formation were confirmed by neutralizing antibody, chemical inhibitors, and fluorescent pathway reporter. In addition, elevated reactive oxygen species (ROS) produced upon protein depletion was required for the activation of IL-6/STAT3 in D5HS. Importantly, a positive feedback loop was found between ROS and IL-6 during tumor sphere formation. The association of ROS/IL-6/STAT3 to the carcinogenesis of human prostate cells was further examined in xenograft tumors and verified by limiting dilution implantations. Collectively, we have for the first time established human prostate tumor–initiating cells based on physiologic adaption. The intrinsic association of ROS and IL-6/STAT3 signaling in human prostate carcinogenesis shed new light on this relationship and define therapeutic targets in this setting. *Cancer Res; 73(23); 7090–100. ©2013 AACR.*

Introduction

Prostate cancer is the most frequently diagnosed malignancy among males in Western countries and is intimately associated with aging (1). Reactive oxygen species (ROS) is one of the major aging-associated influences on prostate carcinogenesis (2). Although recent epidemiologic and clinical studies have linked prostate cancer risk and ROS, the underlying mechanism remains to be elucidated (3).

In prostate cancer research, one of the big obstacles is the lack of relevant preclinical models to understand the mechanism of human prostate carcinogenesis and to develop effective preventive and therapeutic interventions. In the past 40 years, several malignant transformations of human prostate cells have been established by radiation (4) or chemical treatment, such as cadmium (5), *N*-nitroso-*N*-methylurea (6), or introduction of virus elements (7). In patients, however, prostate cancer is unlikely to be caused by exposure to such strong external carcinogens but is considered mainly a disease of aging.

Previously, we have attempted to establish a prostate carcinogenesis model based on physiologic selection and adaption. We started with a human primary prostate basal cell line EP156T that was derived from human prostate benign tissue and immortalized using the human telomerase catalytic subunit (hTERT; ref. 8). Subsequently, nonmalignant mesenchymal EPT1 cells and premalignant EPT2-D5 cells were derived from EP156T cells in a stepwise manner by selection of cells with loss of contact inhibition and evasion of quiescence, respectively (9, 10). EPT2-D5 cells showed several *in vitro* malignant features such as colony formation in soft agar, resistance to apoptosis, and independence of exogenous growth factors. However, EPT2-D5 cells failed to form xenograft tumors following repeated attempts (9), suggesting that additional change is needed to acquire full malignant transformation.

Authors' Affiliations: [1]The Gade Institute, [2]Broegelmann Research Laboratory, Department of Clinical Science, [3]Department of Medicine, University of Bergen; Departments of [4]Microbiology and [5]Pathology, [6]Center for Medical Genetics and Molecular Medicine, Haukeland University Hospital; [7]Kin*N* Therapeutics AS, Bergen, Norway; [8]College of Pharmacy, Second Military Medical University, Shanghai, PR China; [9]Institute of Pathology, University Medical Center Hamburg-Eppendorf, Hamburg, Germany; [10]Zhejiang-California International NanoSystems Institute, Zhejiang University, Hangzhou, PR China; [11]Swedish Medical Center; and [12]Department of Urology, University of Washington, Seattle, Washington

Note: Supplementary data for this article are available at Cancer Research Online (http://cancerres.aacrjournals.org/).

Corresponding Authors: Xi-Song Ke, Laboratory Building, 5th Floor, Haukeland University Hospital, Bergen 5021, Norway. Phone: 47-55584565; Fax: 47-55584565; E-mail: Xisong.Ke@gades.uib.no; and Karl-Henning Kalland. Phone: 47-55584506; E-mail: Kalland@gades.uib.no

doi: 10.1158/0008-5472.CAN-13-1560

Self-sufficiency in growth signals is a classic oncogenic feature of cancer cells (11–13). No type of normal cell can proliferate in culture without supplement of serum or growth factors, whereas cancer cells invariably show greatly reduced dependence on exogenous growth stimulation and uncontrolled proliferation (12, 13). In addition, chemically defined serum-free medium is widely used to enrich and culture tumor-initiating cells (TIC; refs. 14–16). In this work, we attempted to obtain TICs by adapting EPT2-D5 cells in chemically defined medium without any protein component. Surprisingly, numerous tight prostate spheres were generated from single cells in monolayer culture and efficiently established xenograft tumors.

Materials and Methods

Cell culture and reagents

The prostate cell line EPT2-D5 was grown in MCDB153 medium (Biological Ind. Ltd.) supplemented with 1% Minimum Essential Media (MEM) nonessential amino acids solution, 200 nmol/L hydrocortisone, 10 nmol/L triiodothyronine, 5 μg/mL insulin, 5 μg/mL transferrin, 5 μg/mL sodium selenite, 100 ng/mL testosterone, 5 ng/mL EGF, 50 μg/mL bovine pituitary extract (Invitrogen Life Sciences), 100 U/mL penicillin, 100 μg/mL streptomycin, and 5% fetal calf serum (FCS). Prostate cancer PC3 and DU145 cell lines were grown in Ham's F-12 medium and Dulbecco's Modified Eagle's Medium (DMEM; Lonza) containing 10% FCS, respectively. The medium was changed every 3 days. All the cell lines have been tested and authenticated using forensic grade DNA microsatellite analyses, karyotyping, and copy number analyses in parallel with the experiments reported in this work. Lentiviral pGF-STAT3 reporter was a gift from Dr. Yong-Joon Chwae at Ajou University School of Medicine, Korea. Interleukin (IL)-6 protein (H7416) and chemical reagents cryptotanshinone (C5624), FLLL31 (F9057), AG490 (T3434), *N*-acetyl-L-cysteine (A9165), and melatonin (M5250) were products from Sigma-Aldrich. A neutralizing antibody against IL-6 was from Abcam (ab6672).

Generation and passage of D5HS spheres

EPT2-D5 cells were seeded in T75 tissue culture flasks (TPP) to reach 30% confluence. On the second day, the complete medium was removed, and cells were washed twice with PBS and cultured in basic Ham's F-12 medium (Lonza) without serum and any other protein components (protein free medium). The medium was changed every 3 days. When the culture reached confluence, cells were trypsinized and the reaction was quenched by soybean trypsin inhibitor (Invitrogen), the cells were pelleted, resuspended, and split to 2 new flasks. The protein-free medium was changed every 3 days until the spheres were generated about 2 weeks later. To passage the prostate spheres, culture medium was collected in 15-mL centrifuge tubes and kept at room temperature for 10 minutes to let spheres settle down to the bottom of tubes. The upper nine tenths of medium was gently removed, and the remaining lower part contained most of the big spheres (>50 μm in diameter) and was gently centrifuged at 1300 × *g* for 2 minutes. The pelleted spheres were dissociated enzymatically (0.05% trypsin, 0.53 mmol/L EDTA) and mechanically (pipetting). The dissociated cells were analyzed microscopically for single cellularity. The single cells were transferred to and attached in new T75 tissue culture flask. The protein medium was changed every 3 days until new spheres again were generated after around 10 days.

Measurement of ROS in cells

Cells were grown in complete medium or protein-free medium. Production of ROS at various conditions or treatments was measured by incubation with membrane permeable dye 2′,7′-dichlorofluorescein diacetate (DCFDA; Sigma-Aldrich; final concentration 1 μmol/L) for 10 minutes at 37°C. The ROS levels in the cells were determined by fluorescent microscopy or measurement of the fluorescence (excitation 500 and emission 520 nm) using AccuriC6 flow cytometer (Accuri Cytometers, Inc.).

ELISA

Expression levels of IL-6 in cell supernatants were determined using a commercial sandwich ELISA kit (Fisher Thermo Scientific). Cells were cultured for 3 days and the medium was harvested and centrifuged at 1300 × *g* for 5 minutes. The supernatant was used for determination of IL-6 levels according to the manufacturer's protocol.

Western blotting

The levels of expression and phosphorylation of STAT3 protein were determined by Western blotting following the procedures described previously (10). All the antibodies used in Western blotting were products of Abcam with the dilutions as following: anti-phospho-specific STAT3 (Tyr705) (ab76315) 1:10,000; total STAT3 (ab119352) 1:4,000; endogenous control β-actin (ab11003) 1:1,000.

DNA microarray

Total RNA was converted to Cy3-labeled cRNA targets and hybridized to Agilent Whole Human Genome Microarrays 44k (Cat.no. G4112F and G4845A, Agilent Technologies) according to Agilent's instructions. Arrays were scanned using the Agilent Microarray Scanner Bundle. Raw data were imported and analyzed in J-Express software (Molmine, http://www.molmine.com). Mean spot signals were used as intensity measure, the expression data were quantile normalized over the entire arrays and $\log_2$-transformed. Differentially expressed genes were identified using the feature subset selection (FSS) method. Only genes that changed more than 3.0 fold with $P < 0.01$ were considered as differentially expressed.

Reverse transcription and real-time quantitative PCR

Reverse transcription and real-time quantitative PCR (qPCR) were done as described (17). The TaqMan assays used for quantification of human IL-6 (Hs00985639_m1), IL-6R (Hs00169842_m1), and β-actin (Hs99999903_m1) were obtained from Applied Biosystems.

Mass spectrometric analysis

Proteins harvested from serum-free culture were digested with trypsin and analyzed by mass spectrometry following a

protocol described previously (18). Details of mass spectrometric analysis are described in Supplementary Methods.

Xenograft tumor experiment

For subcutaneous tumor formation, BALB/c nude mice were purchased from Shanghai Experimental Animal Center, Chinese Academy of Sciences and maintained under pathogen-free conditions. About 5×10^6 EPT2-D5 or D5H cells or 4×10^3 D5HS spheres were resuspended in 200 μL PBS and injected subcutaneously into BALB/c nude mice. Five mice were used for each cell type. The tumor was removed from sacrificed nude mice when the diameter was about 70 mm. After mechanical (cutting) and enzymatic (collagenase IV for 30 minutes at 37°C) dissociation, the cells were suspended in Ham's F-12 medium containing 5% FCS and plated in tissue culture flasks. The subcutaneous tumor experiment was approved by the Second Military Medical University Committee on Animal Care.

For orthotopic xenograft tumor experiments, NOD/SCID IL2rγnull mice (male, 6–10 weeks old, the Gade Institute, University of Bergen, Bergen, Norway) were used and experiments were approved by the Norwegian Animal Research Authority and conducted according to The European Convention for the Protection of Vertebrates Used for Scientific Purposes. Bioluminescent EPT3 or EPT3-M1 cells were suspended in 50 μL PBS and injected in the left or right ventrolateral lobes of the prostate. Bioluminescence images were conducted 10 minutes following administration of 150 mg/kg D-luciferin (Promega) intraperitoneally. All Optix images were acquired using Optix MX2 Time-Domain Molecular Imager (ART Inc.). or In Vivo MS FX PRO (Carestream Health Inc.) as previously described (19) or Kodak Molecular imaging software (Version 5.0 Carestream Health Inc).

Immunohistochemical examination

Mice were euthanized and sacrificed and tissues were collected by a certified veterinary. Tumor tissues were fixed in neutral-buffered 4% formaldehyde. Paraffin embedding, preparation of sections, staining, and immunohistochemical (IHC) examination were conducted using standard procedures. Briefly, paraffin-embedded tissue slides were deparaffinized and processed for antigen retrieval using PTLink and pretreatment buffer at pH 9.0 (Dako, DK, S2375) and 100°C for 20 minutes. Finished pretreated slides were washed in TBS. Staining was conducted using specific antibodies and a single staining rabbit/mouse kit (Dako Real Envision K5007) using peroxidase/DAB+. Counter staining was carried out by a hematoxylin staining kit. Histologic images were captured using the Qcapture Suite software with a Qimaging Exi Blue camera attached to a Leica DMRBE microscope. The following primary antibodies and dilutions were used for antigen detection in IHC: AE1/AE3 (ab961, Abcam) prediluted; vimentin (ab8545) prediluted; IL-6 (ab6672) 1:400; phospho-STAT3 Y705 (ab76315) 1:100; STAT3 (ab119352) 1:1,600; cyclin D1 (ab10540) 2 μg/mL, and human cell–specific anti-mitochondrion antibody (ab92824, 1:1,000). Inclusion of only the secondary and not the primary antibody in parallel provided negative controls, in addition to differential staining of different neighboring tissue types in the sections.

Statistical analyses

Two-sample *t* tests were used for differences of sphere formation, IL-6, or ROS levels between different groups. ANOVA was used to identify the differentially expressed genes in microarray data.

Microarray data accession number

The gene microarray data are accessible in database ArrayExpress (ID: E-MTAB-1521) according to MIAME guidelines.

Results

EPT2-D5 cells generated spheres in protein free medium

EPT2-D5 cells showed malignant features *in vitro* but failed to form xenograft tumors (9). To further promote malignant cells, we cultured EPT2-D5 cells in chemically defined medium without any protein components. Most EPT2-D5 cells can survive well in protein-free medium, but the growth speed was much slower than under standard culture conditions (9). When cells were split to new flasks after reaching confluence, cells kept growing in monolayer and surprisingly, multiple tight and large spheres (>50 μm in diameter) were generated and detached from the surface in 2 weeks (Fig. 1A and B). The floating spheres were collected and dissociated to single cells (Fig. 1C). These single cells attached efficiently to the surface and expanded well in new tissue culture flasks (Fig. 1D). New spheres were visible again after 5 days and floating spheres could be collected in 10 days (Fig. 1E and F). We named this process attachment sphere cycles and the cells generating these spheres D5HS (Fig. 1G). This D5HS cycle continued for up to 1 year. The attachment of growing spheres to adherent individual cells in monolayer culture showed that these spheres were generated from single cells (Fig. 1H). The remaining cells in the flask continued forming spheres for up to 3 months even when the floating spheres were harvested every third day (Fig. 1I). This indicates that the spheres were indeed generated by cell proliferation and not by cell aggregation and the whole-cell population did not start to generate spheres simultaneously. In the following study, all the D5HS spheres used were newly generated (passage 2). When D5HS cells were cultured in the presence of serum, cells grew only in monolayer and no sphere was generated, showing the indispensability of protein deprivation for sphere generation.

D5HS spheres initiated tumor growth *in vivo*

The formation of spheres is one important feature of TICs *in vitro* (16). We tested the tumorigenicity of newly generated D5HS by subcutaneous injection in BALB/c nude mice. As controls, EPT2-D5 cells grown in complete medium (D5) and EPT2-D5 cells that were adapted to protein-free medium for 3 days (D5H) were also injected in parallel. Significantly, only D5HS spheres efficiently formed large subcutaneous tumors within 12 weeks (Fig. 2A), indicating the tumor initiation ability of D5HS spheres (tumor spheres). Cells recovered from the subcutaneous tumors were named EPT3. To obtain metastatic tumors, luciferase-expressing EPT3 cells were inoculated orthotopically into the prostate of mice. Large primary tumors and extensive abdominal metastasis were found within 6 weeks (Fig. 2B). We confirmed the human origin of the local

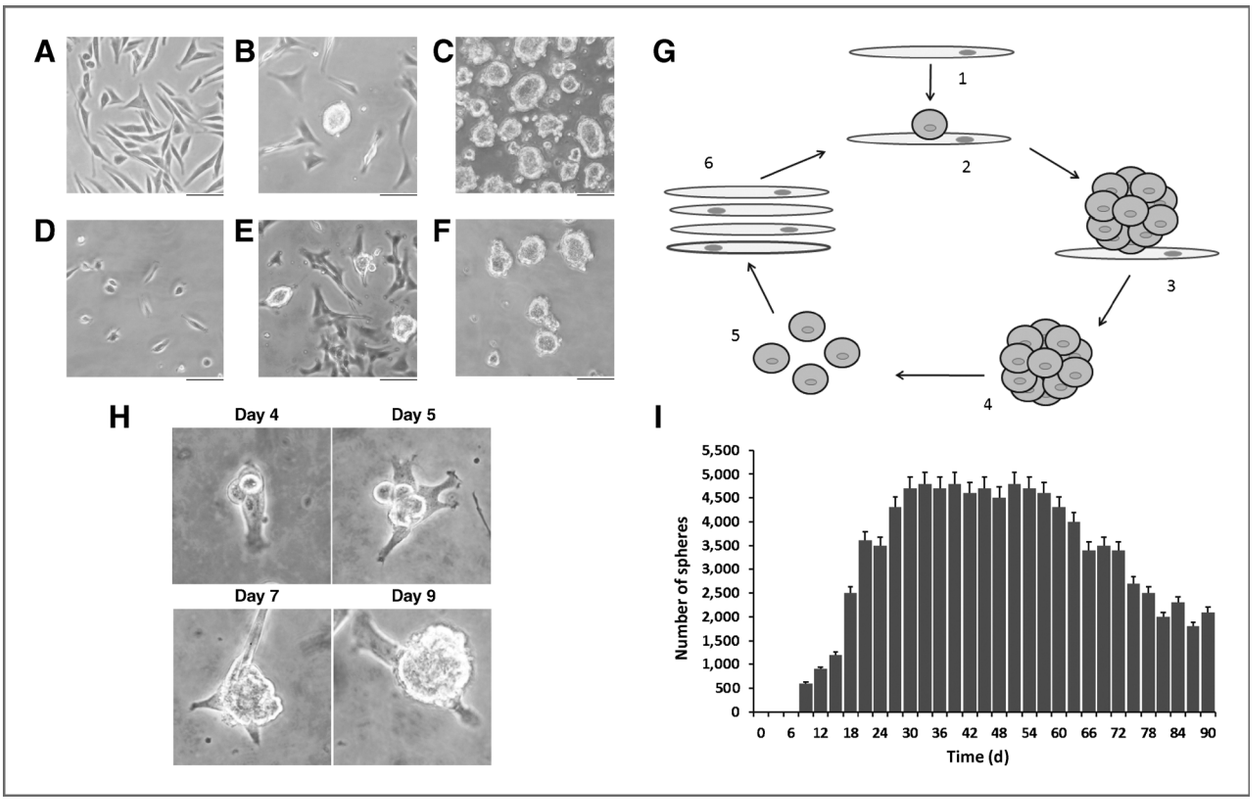

Figure 1. EPT2-D5 generated prostate spheres in protein-free medium. A, EPT2-D5 cells grown in standard medium. B, EPT2-D5 cells were adapted in protein-free medium. Tight and big spheres were generated and floated 10 days following splitting and seeding in new flasks. C, collection of floating spheres from the supernatant of cultures in B. D, prostate spheres were dissociated to single cells and attached in new flasks within 3 hours. E, new spheres were generated from cells in D. F, collected spheres from E. Scale bar, 100 μm. G, a model of the D5HS attachment and sphere formation cycles in monolayer culture. 1, single EPT2-D5 cells in protein-free culture; 2, early stage of sphere formation; 3, later stage of sphere formation; 4, floating spheres; 5, single cells dissociated from spheres; 6, attached single cells in new flask. H, representative figures of growing spheres from single adherent cells at different time points. I, quantification of sphere formation in time course in T75 flasks. Data represent the average of triplicates ± SD.

tumor and metastases by IHC staining using an antibody specific for human mitochondrion (Supplementary Fig. S1). Cells recovered from the primary tumor and the metastases were named EPT3-PT1 and EPT3-M1, respectively. Thereby, we have established a complete and stepwise model of prostate carcinogenesis, which includes prostate primary epithelial EP156T cells, mesenchymal nontransformed EPT1 cells, pre-malignant EPT2 cells, primary tumor derived EPT3-PT1, and metastasis-derived EPT3-M1 cells (Fig. 2C). DNA microsatellite analysis and copy number analysis verified their common genetic origin and a stepwise increase of DNA aberrations in these cells (Supplementary Table S1, Supplementary Data S1 and S2, and Supplementary Fig. S2). The phenotypes that were acquired step by step in the model from EP156T to EPT3-M1 cells are summarized (Fig. 2D).

Activation of autocrine IL-6 in D5HS

To explore the mechanism of sphere formation, we profiled the gene expression of newly generated D5HS using DNA microarrays (Supplementary Data S3). A number of growth factors and cytokines were upregulated in D5HS (Fig. 3A and B). The top 1 increased (98-fold) growth factor gene *IL-6* is particularly interesting, as it is a well-recognized marker of prostate cancer (20–22). The importance of its signaling pathway in D5HS spheres is further supported by the increase of the IL-6 receptor (*IL-6R*; Supplementary Data S3). Real-time qPCR verified the elevated transcription levels of both *IL-6* and *IL-6R* (Fig. 3C). At the protein level, proteomic analysis of the secretome of the D5HS cells detected IL-6 and soluble IL-6 signal transducer IL-6ST (also known as gp130; Fig. 3D and Supplementary Table S2), indicating that the IL-6 signaling is indeed activated in D5HS. ELISA confirmed up to 200-fold higher IL-6 in the culture supernatant of D5HS than in EPT2-D5 and D5H cells (Fig. 3E).

Elevation of IL-6/STAT3 activity was associated with D5HS formation

To test whether elevation of IL-6 is important to sphere formation, a neutralizing antibody against IL-6 was used to treat sphere-forming D5HS cells. Significant decrease of the spheres in treated cells showed the requirement of IL-6 in D5HS generation (Fig. 4A). STAT3 has been reported important in IL-6-type signaling in prostate cancer (19–22). Activated STAT3 signaling in D5HS was verified by Western blotting using an antibody against phosphorylated (Y705) STAT3 (pSTAT3; Fig. 4B). Blockade of IL-6 reduced the pSTAT3 level,

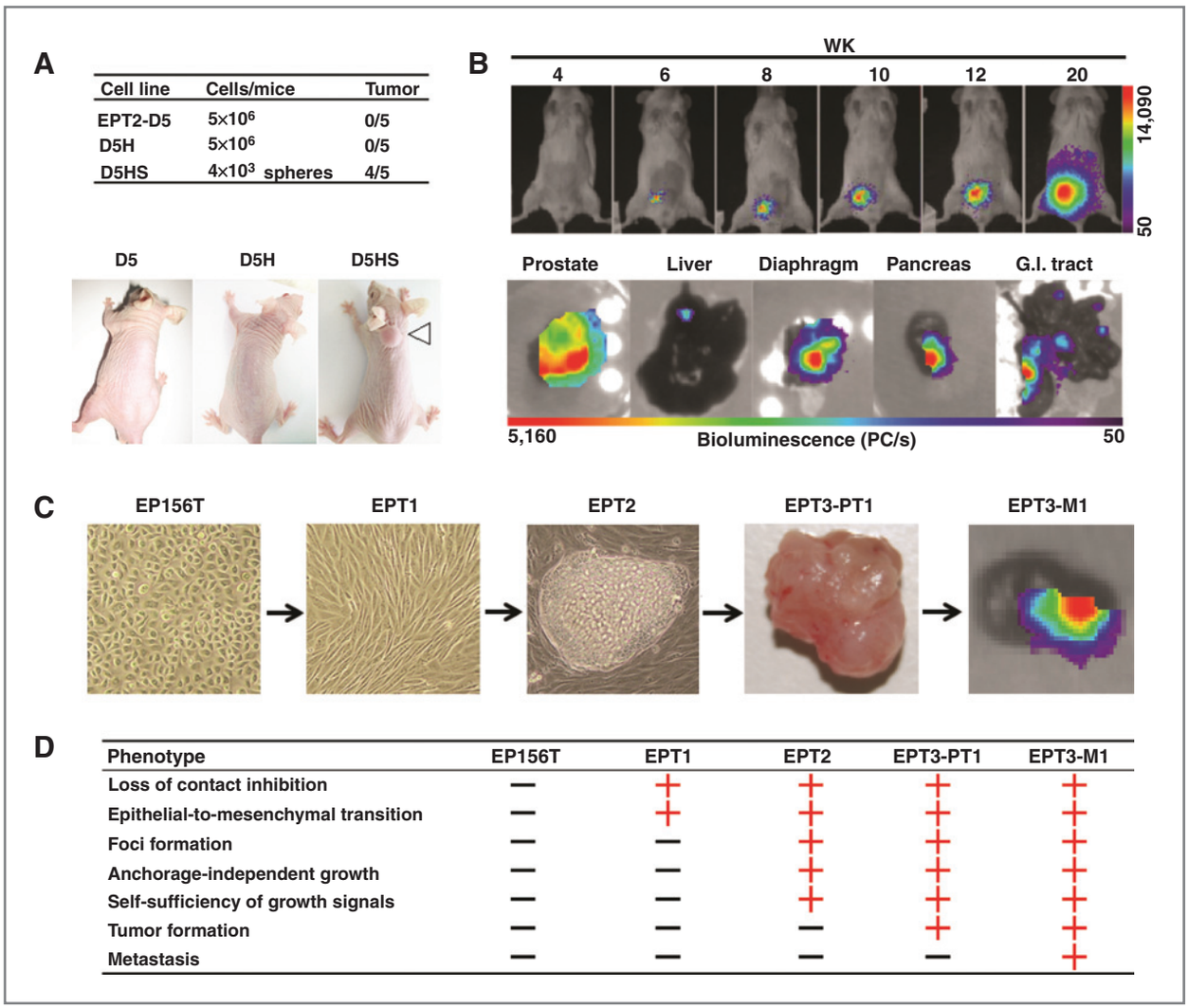

Figure 2. D5HS-initiated subcutaneous tumors and subsequent metastasis *in vivo*. A, examination of tumor formation of EPT2-D5 cells, D5H cells, and D5HS spheres in nude mice. Cells or spheres with indicated numbers were subcutaneously injected into BALB/c nude mice. Five mice were used for each cell type. The representative subcutaneous tumor is shown (arrow). B, cells derived from the subcutaneous tumor in A were orthotopically injected into mice prostate and generated a large primary tumor and extensive metastases in many organs. C, a complete and stepwise prostate carcinogenesis model. EP156T is prostate primary epithelial cells, EPT1 is mesenchymal cells derived from EP156T cells, EPT2 is cloned from foci formed in EPT1 cells, and EPT3-PT1 and EPT3-M1 are derived from a primary tumor in mouse prostate and a pool of abdominal metastases, respectively. The EPT3-M1 panel exhibits a representative pancreatic metastasis shown in B. D, increasingly malignant phenotypes were found in the stepwise carcinogenesis model.

showing IL-6-dependent activation of STAT3 in D5HS (Fig. 4C). To track the STAT3 signaling activity, EPT2-D5 cells were stably transduced with the fluorescence (GFP)-based STAT3 pathway reporter pGF-STAT3. Very few cells expressing GFP showed low activities of STAT3 signaling in EPT2-D5 and D5H cells. A small but distinct subpopulation of GFP-positive cells was found when EPT2-D5 cells started to form spheres in protein-free medium (D5HS; Fig. 4D). Importantly, most of these positive cells were dividing and tending to grow spheres (Fig. 4E). In addition, some of the GFP positive cells divided into one positive and one negative cell (Fig. 4F), suggesting asymmetric division that is a hallmark of self-renewal of cancer stem cells (CSC; ref. 23). D5HS cells with top high ($STAT3^{high}$) and bottom low ($STAT3^{low}$) levels of STAT3 activities were isolated using flow cytometry and sphere formation in $STAT3^{high}$ cells was much higher than in $STAT3^{low}$ cells (Fig. 4G). STAT3 inhibitors significantly reduced the sphere formation in D5HS cells (Fig. 4H), showing the critical role of the STAT3 signaling in D5HS sphere formation. However, the IL-6 level in the supernatant was not significantly affected by these STAT3 inhibitors (Fig. 4I), suggesting that the activation of STAT3 is IL-6-dependent but the activation of IL-6 is not caused by STAT3 signaling activity.

High ROS status was required for IL-6/STAT3 activation in D5HS spheres formation

It has been reported that IL-6/STAT3 signaling can be activated by ROS (24) and that ROS can be generated during

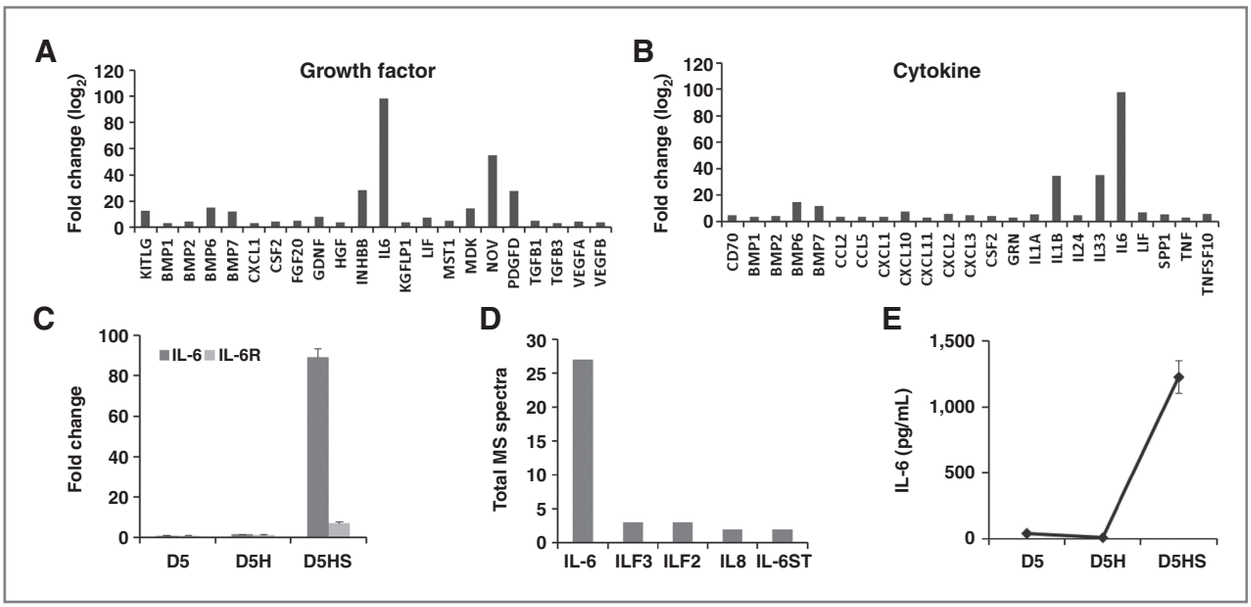

Figure 3. Activated IL-6 in D5HS. A and B, significantly activated growth factors (A) and cytokines (B) in D5HS spheres compared with EPT2-D5 cells based on DNA microarray data. C, examination of the mRNA level of IL-6 and IL-6R by real-time qPCR. D, a bar chart showing the total MS spectrum counts of 5 interleukin-related proteins in the secretome of D5HS spheres. E, examination of IL-6 level in culture supernatant by ELISA. Data represent the average of triplicates ± SD in D and E.

serum deprivation (25). To test the possibility that the activation of IL-6/STAT3 in D5HS is due to ROS induced by growth factor withdrawal, endogenous ROS were detected using redox sensitive dye DCFDA. As presented in Fig. 5A, very few and weak signals were detected in EPT2-D5 cells growing in complete medium, whereas signals were significantly stronger (5-fold) when cells were adapted in protein free medium for 3 days (D5H; Fig. 5A and B). Strikingly, even higher (24-fold) ROS level was found in D5HS (Fig. 5A and B). Treatment of D5HS cells with anti-oxidants *N*-acetyl-L-cysteine (NAC) and melatonin significantly reduced DCFDA levels (Fig. 5C), showing that ROS indeed were induced in EPT2-D5 cells upon growth factor withdrawal. Similar to STAT3-positive cells, heterogeneous intensities of ROS were found among D5HS cells and most cells with higher ROS status tended to generate spheres (Fig. 5A). D5HS cells with top high and bottom low ROS levels were isolated and named ROS^{high} and ROS^{low} cells, respectively. Significantly, ROS^{high} cells generated numerous spheres, whereas ROS^{low} cells continuously grew in monolayer without sphere formation even at day 18 (Fig. 5D and E). Treatment of ROS^{high} cells with antioxidants NAC and melatonin efficiently decreased the sphere numbers (Fig. 5E), showing the indispensable role of ROS in D5HS formation. Examination of secreted IL-6 showed much higher IL-6 in ROS^{high} cells than in ROS^{low} cells (Fig. 5F), and the IL-6 level in ROS^{high} cells can be repressed by NAC and melatonin (Fig. 5F), indicating the requirement of ROS for IL-6 activation in D5HS sphere formation. Consistently, higher STAT3 phosphorylation was found in ROS^{high} cells than in ROS^{low} cells (Fig. 5G), and the level can also be reduced by antioxidant melatonin (Fig. 5G). All these data showed the requirement of ROS for spheres formation and IL-6/STAT3 activation.

It has been reported that ROS were induced in a few hours upon serum starvation and the level was relatively stable or lower afterwards (24). The much higher (4.8-fold) ROS level in D5HS than in D5H cells suggested an additional factor inducing ROS in D5HS (Fig. 5A and B). We tested whether it was due to the highly activated IL-6 considering that cytokines can stimulate intracellular ROS (26). As expected, the ROS level in D5HS was reduced (1.7-fold) by neutralizing antibody against IL-6 (Fig. 5H), and conversely, adapting EPT2-D5 cells in protein-free medium containing IL-6 protein at 2 ng/mL induced significant higher (2.1-fold) ROS level than control cells (Fig. 5I), indicating a positive feedback loop between ROS and IL-6 in D5HS formation. A ROS/IL-6/STAT3 regulation cascade in prostate tumor sphere formation is consequently proposed (Fig. 5J).

IL-6/STAT3 signaling defined TICs in the EPT3 tumor model

To evaluate the IL-6/STAT3 signaling activity in EPT3 tumor formation *in vivo*, the expression of IL-6 and STAT3, as well as a putative STAT3 target cyclin D1, were examined in the xenograft tumors by IHC staining. Clear staining of IL-6 with a pericellular and patchy intercellular pattern was detected in both primary and metastatic tumors (Fig. 6A). pSTAT3 was detected in the nuclei of a small proportion of prostate tumor cells (Fig. 6A). Total STAT3, on the other hand, stained the cytoplasm of a larger proportion of cells in addition to several nuclei (Fig. 6A). Nuclear staining of cyclin D was evident in a proportion of cells (Fig. 6A), all together indicating activation of IL-6/STAT3 signaling in the EPT3 primary tumor and metastasis.

Autocrine IL-6 and phosphorylation of STAT3 were also measured in EPT3 tumor–derived EPT3-PT1 and -M1 cells. The

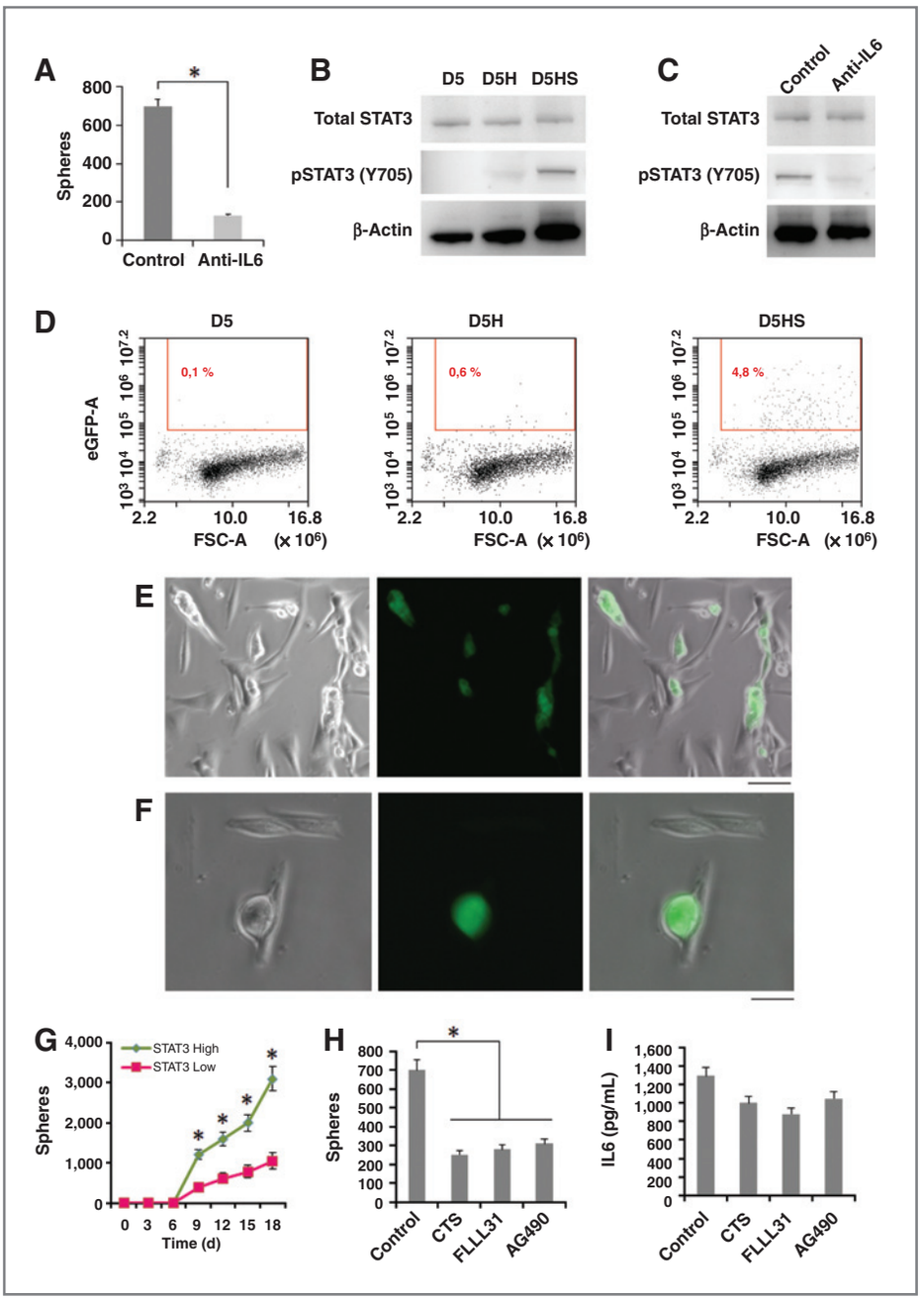

Figure 4. IL-6/STAT3 signaling in D5HS sphere formation. A, single D5HS cells were grown in 6-well plates with protein-free medium containing a neutralizing antibody against IL-6 (1:400 dilution). Spheres were counted at day 18. B, Western blot analysis of phosphorylated (Y705) STAT3 (pSTAT3) in the indicated cells. C, D5HS cells were treated with IL-6 antibody for 18 days and pSTAT3 was examined by Western blotting. D, flow cytometric analysis of GFP-expressing cells that were stably transduced by a GFP-based STAT3 reporter. The percentages of positive cells are indicated. E, among D5HS cells, the GFP-expressing cells (high STAT3 signaling cells) tended to be sphere-forming cells. Scale bar, 50 μm. F, a single D5HS cell was divided into one GFP-positive cell and one GFP-negative cell. Scale bar, 50 μm. G, sphere formation in D5HS cells with top 5% high and bottom 5% low GFP expression levels. Cells were cultured in T75 tissue culture flasks. H and I, D5HS cells in 6-well plates were treated with STAT3 chemical inhibitors cryptotanshinone (CTS; 0.5 μmol/L), FLLL31 (10 μmol/L), and AG490 (10 μmol/L). The medium was changed every 3 days. Spheres (H) and secreted IL-6 (I) were examined at day 18. Data represent the average of triplicates ± SD in A, G, H, and I. *, $P < 0.01$.

levels of secreted IL-6 in both cell lines were in the same range as for D5HS cells and more than 200-fold higher than in EPT2-D5 cells (Fig. 6B). The autocrine effect of IL-6 in EPT3 tumor–derived cells was extremely high considering that these cells were cultured in complete medium without the cell stress experienced by D5HS cells due to protein depletion. Consistently, ROS level in EPT3-M1 cells was also much higher (5-fold) than in EPT2-D5 cells (Fig. 6C and D). In addition, antioxidant melatonin efficiently blocked the production of IL-6 in EPT3-M1 cells (Fig. 6E), indicating that the high level of IL-6 in EPT3 tumors is due to high endogenous ROS, the same as in D5HS. The high level of IL-6/STAT3 signaling in EPT3 tumor cells is also evident compared with DU145 and PC3 cell lines that are widely used for studying the IL-6/STAT3 signaling in prostate cancer (27, 28). The IL-6 level in EPT3-M1 cells are 4- and 2.5-fold higher than in PC3 and DU145 cells, respectively (Fig. 6F). Western blotting also showed higher phosphorylation of STAT3 in EPT3-PT1 and EPT3-M1 cells (Fig. 6G).

To further test the role of IL-6/STAT3 activity in EPT3 tumor initiation, EPT3-M1 cells were transduced with the STAT3–GFP reporter and the top and bottom 5% of GFP expressed cells ($STAT3^{high}$ and $STAT3^{low}$) were examined in mice. As few as 500 $STAT3^{high}$ cells efficiently generated large tumors in 7 weeks, whereas many more $STAT3^{low}$ cells were needed to

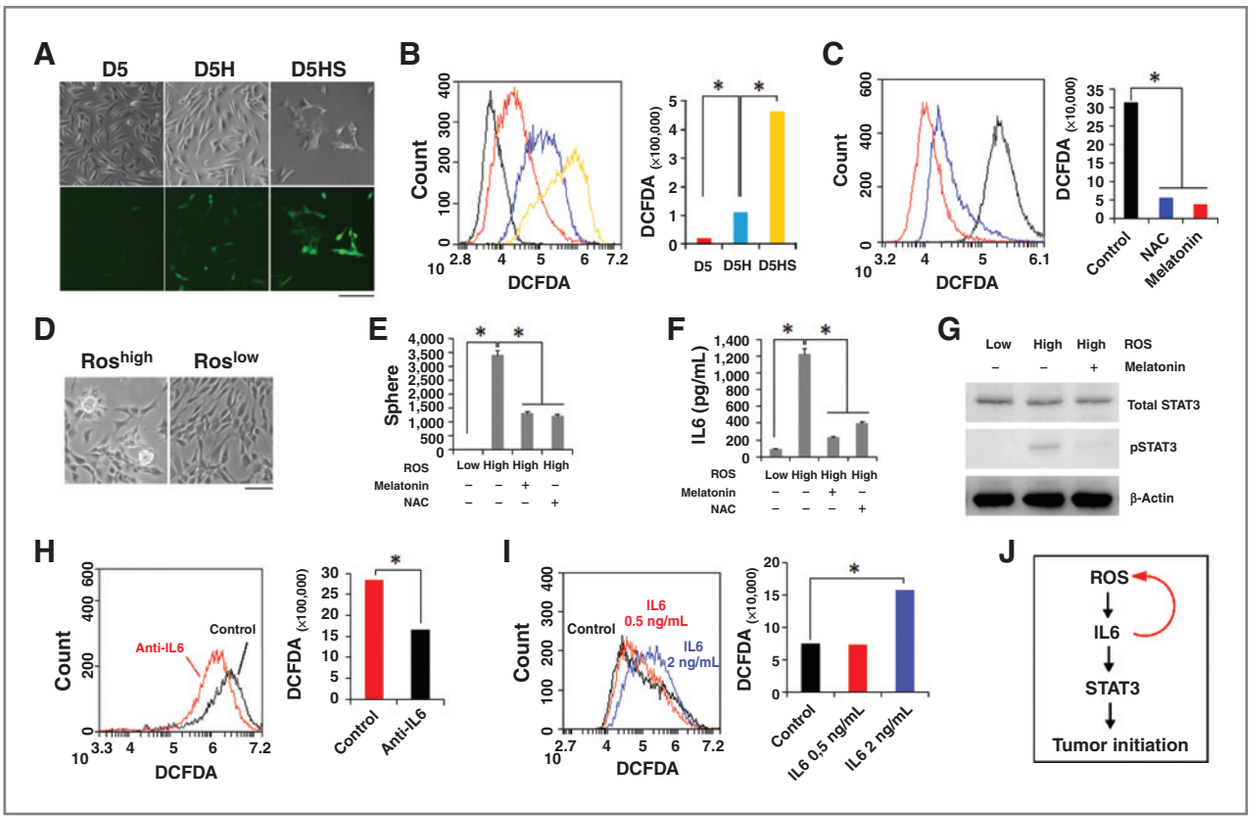

Figure 5. Association of ROS and IL-6/STAT3 activation and sphere formation in D5HS cells. A, fluorescent images of ROS levels in indicated cells by DCFDA assay. Scale bar, 50 μm. B, flow cytometric analysis of ROS levels of D5 (red), D5H (blue), and D5HS (yellow) cells in A; D5 cells without incubation with DCFDA (black) was included as control. The mean values of DCFDA in D5, D5H, and D5HS cells are shown. C, flow cytometric analysis of ROS levels in D5HS treated with vehicle (black) or antioxidants 100 μmol/L melatonin (red) and 2 mmol/L NAC (blue) for 48 hours. The mean values of DCFDA are shown. D, D5HS cells with top 10% high and bottom 10% low ROS levels showed difference in sphere formation. Scale bar, 50 μm. E and F, examination of sphere formation (E) and IL-6 levels (F) in ROS^{low} and ROS^{high} cells, as well as ROS^{high} cells treated with 2 mmol/L NAC and 100 μmol/L melatonin for 18 days. G, examination of phosphorylated STAT3 (pSTAT3) levels in ROS^{low}, ROS^{high} with and without treatment of 100 μmol/L melatonin for 18 days. H, ROS levels in D5HS cells treated with IL-6 antibody (1:400 dilution) for 18 days. The mean values of DCFDA intensities are shown. I, ROS levels in EPT2-D5 cells adapted in basic Ham's medium (control) or addition of IL-6 protein 48 hours. The mean values of DCFDA are shown. J, a ROS/IL-6/STAT3 cascade is proposed in D5HS sphere formation in protein-free culture. A positive feedback loop between ROS and IL-6 is found in the cascade. Data represent the average of triplicates ± SD in E and F. *, $P < 0.01$.

form tumors and metastasis (Fig. 6H), showing the high tumorigenicity of $STAT3^{high}$ cells.

Discussion

In this work, we have generated prostate TICs via adapting premalignant EPT2 cells in protein-free medium. Chemically defined serum-free medium is widely used to culture tumor spheres or TICs (14–16). However, these media are often supplemented with growth factors such as EGF and fibroblast growth factor (FGF), and all cells are cultured in nonadherent conditions (14–16). In the current study, EPT2-D5 cells efficiently generated tumor spheres in medium completely free of serum or any other growth factor, suggesting an even higher independence of exogenous growth stimulation. In addition, generation of D5HS spheres from single adherent cells provides a unique model to study the cell division and metabolism of TICs.

Although ROS and cellular oxidant stress have long been associated with cancer, and elevated ROS level is a hallmark of many highly invasive cancers (29, 30), there is a hypothesis that keeping ROS levels low within stem cells or TICs is an important feature of "stemness" and offers protection against the cell toxicities of ROS (31, 32). Recent studies suggest that ROS not only are byproducts of cellular metabolism but also play roles as second messengers in cell signaling (33). In this work, high ROS level is indispensable to tumor sphere formation, autocrine activity of IL-6, and activation of STAT3 signaling, showing the central role of ROS as second messenger in tumor initiation. The different requirements of ROS in stem cells and D5HS cells may due to their different status: the relatively quiescent state of stem cells under normal circumstances is in contrast to the uncontrolled proliferation of tumor spheres with high ROS status advantageous for high proliferation. Similarly, high ROS supported proliferation, self-renewal, and neurogenesis of neural stem and progenitor

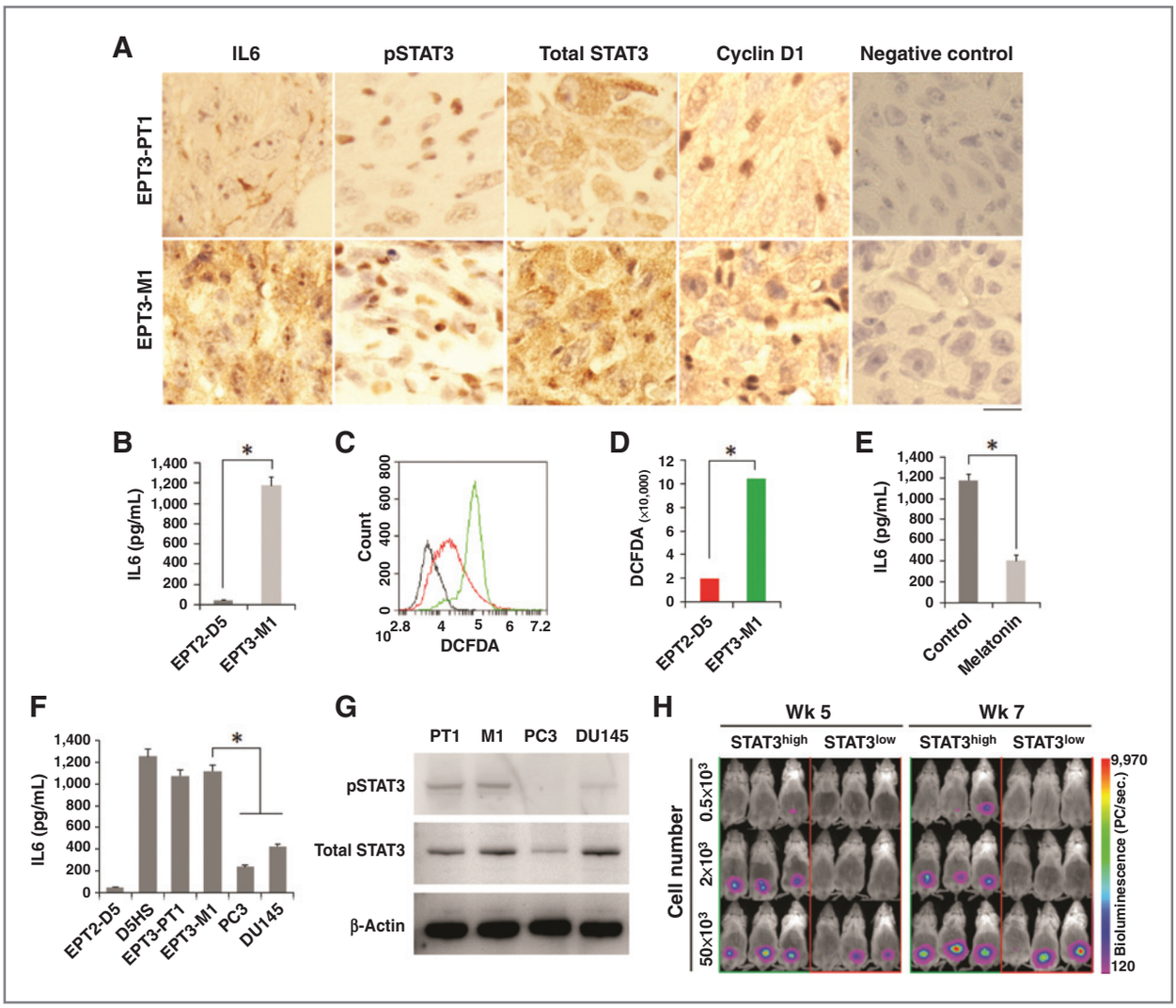

Figure 6. Activation of ROS/IL-6/STAT3 signaling in EPT3 tumor initiation and metastasis. A, IHC staining of IL-6, phosphorylated STAT3, total STAT3, and cyclin D1 in primary tumor EPT3-PT1 and metastasis EPT3-M1. Scale bar, 10 μm. B, examination of secreted IL-6 levels in EPT2-D5 and EPT3-M1 cells by ELISA. C, flow cytometric analysis of ROS levels of EPT2-D5 (red) and EPT3-M1 (green) cells. EPT2-D5 cells without incubation with DCFDA (black) were included as control. D, quantification of the ROS intensities of cells in C; data show mean values of DCFDA signal. E, ELISA examination of secreted IL-6 level in EPT3-M1 cells treated with melatonin (100 μmol/L) for 3 days. F, comparison of IL-6 levels between cells in this model and prostate cancer cell lines PC3 and DU145. G, Western blotting of phosphorylated STAT3 in EPT3-PT1 (PT1), EPT3-M1 (M1), and prostate cancer cell lines PC3 and DU145. H, EPT3-M1 cells with top 5% high and bottom 5% low STAT3 signaling activities were isolated by flow cytometry and orthotopically injected into mice prostate. The cell numbers of each group are shown. Bioluminescent images were acquired at week 5 and 7. Data represent the average of triplicates ± SD in B, E, and F. *, $P < 0.01$.

cells (34), suggesting the context-dependent and complex function of ROS in stem cells and TICs. Actually, tumor spheres and TICs were usually maintained in serum-free medium *in vitro* (14–16). The absence of serum inevitably induces high ROS status in these cultures, which indicates that higher ROS level is common in tumor spheres and TICs.

IL-6 is elevated in the sera of patients with metastatic prostatic cancer and it is a widely recognized marker of prostate cancer (20–22, 35). Extensive studies have shown the central role of STAT3 in IL-6-type cytokine signaling in prostate cancer (27, 28, 36). Using a STAT3 reporter, we found that the IL-6-dependent STAT3-positive cells are enriched in tumor sphere–forming cells, and the top STAT3-positive cells isolated from xenograft tumors showed much stronger tumorigenicity than negative control cells *in vivo*, showing the essential role of IL-6/STAT3 activity in prostate tumor initiation. The central role of IL-6 in tumor initiation is also found in recent reports on prostate and breast cancer. Expression of IL-6 is much higher in prostate CSCs than non–stem cancer cells (NSCC) and NSCCs can be converted to CSCs by IL-6 treatment (37). Although these prostate CSCs were defined by cell surface markers CD44+/CD133+ (37), whereas our prostate TICs were defined by the activity of STAT3 signaling, both showed high

dependence on IL-6. Activation of an IL-6 inflammatory loop is required for expanding the trastuzumab-resistant breast CSC population (38). However, it should be noted that other pathways or factors are also important to the D5HS generation and tumor initiation as not all the sphere-forming cells scored positive for STAT3 signaling (Fig. 4G) and chemical blockade of STAT3 signaling did not abolish all sphere formation (Fig. 4H), and finally, $STAT3^{low}$ cells still generated tumors even though many more cells were needed (Fig. 6H). It will be interesting to evaluate the roles of other growth factors and cytokines that were also significantly increased in D5HS, such as bone morphogenetic protein (BMP), platelet-derived growth factor (PDGF), TGFBs, VEGFs, IL8, and IL33 (Fig. 3A and B).

As discussed above, there are abundant epidemiologic and clinical studies indicating the correlation of prostate cancer to ROS and IL-6/STAT3 signaling, respectively. In this study, for the first time, we linked an intrinsic association of ROS and IL-6/STAT3 in prostate carcinogenesis, which allows an improved therapeutic strategy regarding prostate cancer. Importantly, we observed a positive feedback loop between ROS and IL-6 during prostate tumor sphere formation. Induction of IL-6 by ROS was previously reported in many contexts (39–41). The mechanisms involved were transcriptional activation of the IL-6 gene through an NF-κB–dependent pathway (39, 40) or mitogen-activated protein kinase (MAPK) activity (41). On the other hand, IL-6 has been reported to induce ROS by activating the transcription and enzyme activity of spermine oxidase (SMO), which oxidizes spermine into spermidine, 3-aminopropanal, and H_2O_2 (42). Spermine can also be first acetylated by spermidine/spermine *N*1-acetyltransferase (SAT) and then oxidized by *N*1-acetylpolyamine oxidase (APAO), producing H_2O_2 as a byproduct (42). The expression of the SAT gene is significantly (5.5-fold) increased in D5HS (Supplementary Data S3), which can be a potential mechanism of the induction of ROS by IL-6 in D5HS.

Disclosure of Potential Conflicts of Interest

No potential conflicts of interest were disclosed.

Authors' Contributions

Conception and design: Y. Qu, A.M. Oyan, E. McCormack, K.-H. Kalland, X.-S. Ke

Development of methodology: Y. Qu, A.M. Oyan, M. Popa, W. Zhang, E. McCormack, K.-H. Kalland, X.-S. Ke

Acquisition of data (provided animals, acquired and managed patients, provided facilities, etc.): A.M. Oyan, R. Liu, Y. Hua, J. Zhang, R. Hovland, K.A. Brokstad, R. Simon, A. Molven, W. Zhang, E. McCormack, K.-H. Kalland, X.-S. Ke

Analysis and interpretation of data (e.g., statistical analysis, biostatistics, computational analysis): Y. Qu, A.M. Oyan, R. Hovland, M. Popa, A. Molven, B. Lin, E. McCormack, K.-H. Kalland, X.-S. Ke

Writing, review, and/or revision of the manuscript: Y. Qu, A.M. Oyan, R. Hovland, K.A. Brokstad, A. Molven, B. Lin, W. Zhang, E. McCormack, K.-H. Kalland, X.-S. Ke

Administrative, technical, or material support (i.e., reporting or organizing data, constructing databases): M. Popa, X. Liu, K.A. Brokstad, W. Zhang, K.-H. Kalland, X.-S. Ke

Study supervision: E. McCormack, K.-H. Kalland, X.-S. Ke

Acknowledgments

The authors thank Dr. Yong-Joon Chwae for providing the STAT3 reporter pGF1-STAT3; Beth Johannessen for cell culture work; Hua My Hoang for DNA microarray profiling; and Anne Aarsand, Marianne Eidsheim, Kjerstin Jakobsen, and Dagny Ann Sandnes for tissue embedding, sectioning, and immunohistochemistry. They also thank Marianne Enger for flow cytometry and cell sorting, Solrun Steine for DNA microsatellite analyses, and Kjetil Solland and Atle Brendehaug for chromosome analyses and the Molecular Imaging Centre (MIC) in University of Bergen for advanced microscopy. They thank Dr. Huarong Zhang and Yingying Ma for help in the mass spectrometry analysis and Kjell Petersen at the Elixir.no bioinformatics helpdesk, funded by the Research Council of Norway through the Large Infrastructure program, for microarray data management and export to the public data repository Array Express.

Grant Support

This work was supported by grants from Helse Vest (911626, 911555, 911747, 911582), the Bergen Medical Research Foundation, Bergen Research Foundation, the Norwegian Cancer Society, Chinese NSFC (81230090), MOST of China (2012AA022705), EU FP7- PEOPLE-IRSES-2008 (TCMCANCER Project 230232 and PPI-MARKER 247097).

Received June 4, 2013; revised August 22, 2013; accepted September 17, 2013; published OnlineFirst October 7, 2013.

References

1. Hsing AW, Tsao L, Devesa SS. International trends and patterns of prostate cancer incidence and mortality. Int J Cancer 2000;85:60–7.
2. Bostwick DG, Alexander EE, Singh R, Shan A, Qian J, Santella RM, et al. Antioxidant enzyme expression and reactive oxygen species damage in prostatic intraepithelial neoplasia and cancer. Cancer 2000;89:123–34.
3. Khandrika L, Kumar B, Koul S, Maroni P, Koul HK. Oxidative stress in prostate cancer. Cancer Lett 2009;282:125–36.
4. Kuettel MR, Thraves PJ, Jung M, Varghese SP, Prasad SC, Rhim JS, et al. Radiation-induced neoplastic transformation of human prostate epithelial cells. Cancer Res 1996;56:5–10.
5. Achanzar WE, Diwan BA, Liu J, Quader ST, Webber MM, Waalkes MP. Cadmium-induced malignant transformation of human prostate epithelial cells. Cancer Res 2001;61:455–8.
6. Rhim JS, Jin S, Jung M, Thraves PJ, Kuettel MR, Webber MM, et al. Malignant transformation of human prostate epithelial cells by N-nitroso-N-methylurea. Cancer Res 1997;57:576–80.
7. Rhim JS, Webber MM, Bello D, Lee MS, Arnstein P, Chen LS, et al. Stepwise immortalization and transformation of adult human prostate epithelial cells by a combination of HPV-18 and v-Ki-ras. Proc Natl Acad Sci U S A 1994;91:11874–8.
8. Kogan I, Goldfinger N, Milyavsky M, Cohen M, Shats I, Dobler G, et al. hTERT-immortalized prostate epithelial and stromal-derived cells: an authentic *in vitro* model for differentiation and carcinogenesis. Cancer Res 2006;66:3531–40.
9. Ke XS, Li WC, Hovland R, Qu Y, Liu RH, McCormack E, et al. Reprogramming of cell junction modules during stepwise epithelial to mesenchymal transition and accumulation of malignant features *in vitro* in a prostate cell model. Exp Cell Res 2011;317:234–47.
10. Ke XS, Qu Y, Goldfinger N, Rostad K, Hovland R, Akslen LA, et al. Epithelial to mesenchymal transition of a primary prostate cell line with switches of cell adhesion modules but without malignant transformation. PLoS One 2008;3:e3368.
11. Cross M, Dexter TM. Growth factors in development, transformation, and tumorigenesis. Cell 1991;64:271–80.
12. Hanahan D, Weinberg RA. The hallmarks of cancer. Cell 2000;100:57–70.
13. Hanahan D, Weinberg RA. Hallmarks of cancer: the next generation. Cell 2011;144:646–74.
14. Singh SK, Clarke ID, Terasaki M, Bonn VE, Hawkins C, Squire J, et al. Identification of a cancer stem cell in human brain tumors. Cancer Res 2003;63:5821–8.

15. Ponti D, Costa A, Zaffaroni N, Pratesi G, Petrangolini G, Coradini D, et al. Isolation and *in vitro* propagation of tumorigenic breast cancer cells with stem/progenitor cell properties. Cancer Res 2005;65: 5506–11.
16. Ricci-Vitiani L, Lombardi DG, Pilozzi E, Biffoni M, Todaro M, Peschle C, et al. Identification and expansion of human colon-cancer-initiating cells. Nature 2007;445:111–5.
17. Ke XS, Qu Y, Cheng Y, Li WC, Rotter V, Oyan AM, et al. Global profiling of histone and DNA methylation reveals epigenetic-based regulation of gene expression during epithelial to mesenchymal transition in prostate cells. BMC Genomics 2010;11:669.
18. Stewart JJ, White JT, Yan X, Collins S, Drescher CW, Urban ND, et al. Proteins associated with Cisplatin resistance in ovarian cancer cells identified by quantitative proteomic technology and integrated with mRNA expression levels. Mol Cell Proteomics 2006;5:433–43.
19. McCormack E, Silden E, West RM, Pavlin T, Micklem DR, Lorens JB, et al. Nitroreductase, a near-infrared reporter platform for *in vivo* time-domain optical imaging of metastatic cancer. Cancer Res 2013;73: 1276–86.
20. Twillie DA, Eisenberger MA, Carducci MA, Hseih WS, Kim WY, Simons JW. Interleukin-6: a candidate mediator of human prostate cancer morbidity. Urology 1995;45:542–9.
21. Drachenberg DE, Elgamal AA, Rowbotham R, Peterson M, Murphy GP. Circulating levels of interleukin-6 in patients with hormone refractory prostate cancer. Prostate 1999;41:127–33.
22. Smith PC, Hobisch A, Lin DL, Culig Z, Keller ET. Interleukin-6 and prostate cancer progression. Cytokine Growth Factor Rev 2001;12: 33–40.
23. Knoblich JA. Mechanisms of asymmetric stem cell division. Cell 2008;132:583–97.
24. Yoon S, Woo SU, Kang JH, Kim K, Kwon MH, Park S, et al. STAT3 transcriptional factor activated by reactive oxygen species induces IL6 in starvation-induced autophagy of cancer cells. Autophagy 2010;6: 1125–38.
25. Pandey S, Lopez C, Jammu A. Oxidative stress and activation of proteasome protease during serum deprivation-induced apoptosis in rat hepatoma cells; inhibition of cell death by melatonin. Apoptosis 2003;8:497–508.
26. Lo YY, Wong JM, Cruz TF. Reactive oxygen species mediate cytokine activation of c-Jun NH2-terminal kinases. J Biol Chem 1996;271: 15703–7.
27. Mora LB, Buettner R, Seigne J, Diaz J, Ahmad N, Garcia R, et al. Constitutive activation of Stat3 in human prostate tumors and cell lines: direct inhibition of Stat3 signaling induces apoptosis of prostate cancer cells. Cancer Res 2002;62:6659–66.
28. Barton BE, Karras JG, Murphy TF, Barton A, Huang HF. Signal transducer and activator of transcription 3 (STAT3) activation in prostate cancer: direct STAT3 inhibition induces apoptosis in prostate cancer lines. Mol Cancer Ther 2004;3:11–20.
29. Szatrowski TP, Nathan CF. Production of large amounts of hydrogen peroxide by human tumor cells. Cancer Res 1991;51:794–8.
30. Grek CL, Tew KD. Redox metabolism and malignancy. Curr Opin Pharmacol 2010;10:362–8.
31. Smith J, Ladi E, Mayer-Proschel M, Noble M. Redox state is a central modulator of the balance between self-renewal and differentiation in a dividing glial precursor cell. Proc Natl Acad Sci U S A 2000;97:10032–7.
32. Diehn M, Cho RW, Lobo NA, Kalisky T, Dorie MJ, Kulp AN, et al. Association of reactive oxygen species levels and radioresistance in cancer stem cells. Nature 2009;458:780–3.
33. Reuter S, Gupta SC, Chaturvedi MM, Aggarwal BB. Oxidative stress, inflammation, and cancer: how are they linked? Free Radic Biol Med 2010;49:1603–16.
34. Le Belle JE, Orozco NM, Paucar AA, Saxe JP, Mottahedeh J, Pyle AD, et al. Proliferative neural stem cells have high endogenous ROS levels that regulate self-renewal and neurogenesis in a PI3K/Akt-dependant manner. Cell Stem Cell 2011;8:59–71.
35. Adler HL, McCurdy MA, Kattan MW, Timme TL, Scardino PT, Thompson TC. Elevated levels of circulating interleukin-6 and transforming growth factor-beta1 in patients with metastatic prostatic carcinoma. J Urol 1999;161:182–7.
36. Lou W, Ni Z, Dyer K, Tweardy DJ, Gao AC. Interleukin-6 induces prostate cancer cell growth accompanied by activation of stat3 signaling pathway. Prostate 2000;42:239–42.
37. Iliopoulos D, Hirsch HA, Wang G, Struhl K. Inducible formation of breast cancer stem cells and their dynamic equilibrium with non-stem cancer cells via IL6 secretion. Proc Natl Acad Sci USA 2011;108:1397–402.
38. Korkaya H, Kim GI, Davis A, Malik F, Henry NL, Ithimakin S, et al. Activation of an IL6 inflammatory loop mediates trastuzumab resistance in HER2+ breast cancer by expanding the cancer stem cell population. Mol Cell 2012;47:570–84.
39. Kosmidou I, Vassilakopoulos T, Xagorari A, Zakynthinos S, Papapetropoulos A, Roussos C. Production of interleukin-6 by skeletal myotubes: role of reactive oxygen species. Am J Respir Cell Mol Biol 2002;26:587–93.
40. Simeonova PP, Toriumi W, Kommineni C, Erkan M, Munson AE, Rom WN, et al. Molecular regulation of IL-6 activation by asbestos in lung epithelial cells: role of reactive oxygen species. J Immunol 1997; 159:3921–8.
41. Junn E, Lee KN, Ju HR, Han SH, Im JY, Kang HS, et al. Requirement of hydrogen peroxide generation in TGF-beta 1 signal transduction in human lung fibroblast cells: involvement of hydrogen peroxide and Ca2+ in TGF-beta 1-induced IL-6 expression. J Immunol 2000;165: 2190–7.
42. Babbar N, Hacker A, Huang Y, Casero RA Jr. Tumor necrosis factor alpha induces spermidine/spermine N1-acetyltransferase through nuclear factor kappaB in non-small cell lung cancer cells. J Biol Chem 2006;281:24182–92.